# Low frequency behaviour of the subsonic doublet lattice method

**L. van Zyl**
Defencetek
Pretoria
South Africa

## ABSTRACT

The results of the subsonic doublet lattice method (DLM), i.e. generalised unsteady aerodynamic forces (GAFs) at a set of reduced frequencies, are often used as input to the solution of the flutter equation. Solutions of the flutter equation are usually required at many more reduced frequencies than GAFs are calculated for by the DLM and some form of interpolation is therefore required. In the *p*-*k* formulation of Rodden, Harder and Bellinger, the imaginary part of the GAFs appear as $Q^I/k$, i.e. the imaginary part of the GAFs divided by the reduced frequency. In the case of real (i.e. non-oscillatory) roots of the flutter equation, the solution is determined entirely by the steady GAFs and the limiting value of $Q^I/k$ at zero frequency. This is also true of the *g*-method of flutter solution as the two formulations are equivalent at $k = 0$. Expressions are derived for calculating the limiting values of $Q^I/k$ directly from the DLM, thereby making the real roots independent of the interpolation of the GAFs. The exact way in which the low frequency DLM results are interpolated has a small effect on the interpolation quality in the case of the *p*-*k* flutter equation, whereas it has a significant qualitative effect on the results of the *g*-method of flutter solution of Chen.

## NOMENCLATURE

| | |
|---|---|
| $b$ | reference length, usually mean semi-chord |
| $[\mathbf{B}]$ | modal damping matrix |
| $\{C_p\}$ | pressure coefficient distribution, $\{C_p^R\} + i\{C_p^I\}$ |
| $\{C_p^R\}$ | real part of the pressure coefficient distribution |
| $\{C_p^I\}$ | imaginary part of the pressure coefficient distribution |
| $[\mathbf{D}]$ | downwash matrix, $[\mathbf{D^R}]+i[\mathbf{D^I}]$ |
| $[\mathbf{D^R}]$ | real part of the downwash matrix |
| $[\mathbf{D^I}]$ | imaginary part of the downwash matrix |
| $D_{1rs}$ | planar part of the incremental downwash factor |
| $e$ | aerodynamic strip semi-width |
| $k$ | reduced frequency, $\omega b/U$ |
| $k_1$ | $\omega r_1/U$ |
| $[\mathbf{K}]$ | modal stiffness matrix |
| $K_1$ | factor in numerator of planar kernel |
| $K_{10}$ | steady part of the planar kernel function |
| M | Mach number |
| $[\mathbf{M}]$ | modal mass matrix |
| $p$ | differential operator d/d$t$ |
| $[\mathbf{Q}]$ | matrix of generalised unsteady aerodynamic forces, $[\mathbf{Q^R}]+i[\mathbf{Q^I}]$ |
| $[\mathbf{Q^R}]$ | real part of $\mathbf{Q}$ |
| $[\mathbf{Q^I}]$ | imaginary part of $\mathbf{Q}$ |
| $r_1$ | radial distance from sending point to receiving point |
| $T_1$ | direction cosine function |
| $U$ | air speed |
| $\bar{x}$ | streamwise distance from doublet line midpoint to receiving point |
| $\{w\}$ | downwash distribution, |
| $\{W^R\}$ | real part of the downwash distribution |
| $\{W^I\}$ | imaginary part of the downwash distribution divided by $w_r$ |
| $\beta$ | $\sqrt{1-M^2}$ |
| $\Delta x_s$ | box chord length |
| $\lambda_s$ | doublet line sweep angle |
| $\rho$ | air density |
| $\omega$ | angular frequency, Im($p$) |
| $\omega_r$ | wave number, $\omega/U$ |

**Paper No. 2865**. Manuscript received 25 November 2003, revised version received 17 December 2004, accepted 1 April 2005.

https://doi.org/10.1017/S0001924000000749 Published online by Cambridge University Press

## 1.0 INTRODUCTION

The general form of the flutter equation is

$$\left[[\mathbf{M}]p^2+[\mathbf{B}]p+[\mathbf{K}]-\tfrac{1}{2}\rho V^2\left[\mathbf{Q}\left(pb/U\right)\right]\right]\{q\}=0 \qquad \ldots (1)$$

The problem with solving this form of the flutter equation is that the aerodynamic coefficients are generally only available for harmonic motion. The *p-k* formulations of Hassig[1] and Rodden, Harder and Bellinger[2] differ in the approximation to the generalised aerodynamic forces for non-harmonic motion. In Hassig's form it is assumed that the aerodynamic coefficients for harmonic motion are also valid for slowly decaying or growing oscillations, leading to the equation of motion

$$\left[[\mathbf{M}]p^2+[\mathbf{B}]p+[\mathbf{K}]-\tfrac{1}{2}\rho U^2\left[\mathbf{Q}\left(ik\right)\right]\right]\{q\}=0 \qquad \ldots (2)$$

Rodden, Harder and Bellinger divided the aerodynamic matrix into an aerodynamic stiffness matrix and an aerodynamic damping matrix, so that the approximation reads

$$Q\left(pb/U\right)\approx \mathrm{Re}\left(Q\left(ik\right)\right)+\frac{pb}{kU}\mathrm{Im}\left(Q\left(ik\right)\right) \qquad \ldots (3)$$

This approximation leads to the equation of motion

$$\begin{bmatrix}[\mathbf{M}]p^2+\left([\mathbf{B}]-\tfrac{1}{2}\rho bU\,\mathrm{Im}\left(\mathbf{Q}\left(ik\right)\right)/k\right)p\\+[\mathbf{K}]-\tfrac{1}{2}\rho U^2\,\mathrm{Re}\left(Q\left(ik\right)\right)\end{bmatrix}\{q\}=0 \qquad \ldots (4)$$

This equation is always a real general eigenvalue problem, with the roots being either real or complex conjugate pairs.

The aerodynamic approximation used in the *g*-method of Chen[3] is a first-order expansion from the imaginary axis, *viz*

$$Q\left(p\right)\approx Q\left(ik\right)+\left(\frac{pb}{U}-ik\right)\frac{\mathrm{d}\left(Q\left(ik\right)\right)}{\mathrm{d}(ik)} \qquad \ldots (5)$$

leading to the equation of motion

$$\begin{bmatrix}[\mathbf{M}]p^2+\left([\mathbf{B}]+\tfrac{i}{2}\rho Ub\frac{\mathrm{d}\left(\mathbf{Q}\left(ik\right)\right)}{\mathrm{d}k}\right)p\\+[\mathbf{K}]-\tfrac{1}{2}\rho U^2\left[\mathbf{Q}\left(ik\right)-k\frac{\mathrm{d}\left(Q\left(ik\right)\right)}{\mathrm{d}k}\right]\end{bmatrix}\{q\}=0 \qquad \ldots (6)$$

For real roots, i.e. $k = 0$, both Equations (4) and (6) reduce to

$$\begin{bmatrix}[\mathbf{M}]p^2+\left([\mathbf{B}]-\tfrac{1}{2}\rho Ub\frac{\mathrm{d}\left(\mathrm{Im}\left(Q\left(ik\right)\right)\right)}{\mathrm{d}k}\Big|_{k=0}\right)p\\+[\mathbf{K}]-\tfrac{1}{2}\rho U^2Q\left(0\right)\end{bmatrix}\{q\}=0 \qquad \ldots (7)$$

If Equation (7) has real roots, they are valid roots of the flutter equation. The roots of Equation (7) depend only on the values and slopes of the GAFs at $k = 0$. It should be noted that, if the real part of $\mathrm{d}Q/\mathrm{d}k$ was non-zero at $k = 0$ in Equation (6), the simplification to Equation (7) would not be valid. The eigenvalue problem at $k = 0$ would be a complex general eigenvalue problem with the only possible real solution being $p = 0$. Theoretically the real part of the GAFs are smooth and symmetric with respect to $k$ at $k = 0$, however, the solutions to Equations (4) or (6) are generally determined using numerical values of the GAFs calculated by the DLM[4,5] or similar methods. The symmetry and smoothness condition on the real part of the GAFs needs to be enforced in the interpolation scheme for consistency and to obtain a smooth transition from oscillatory to non-oscillatory roots in cases involving static divergence.

The MSC/NASTRAN interpolation scheme[6] applies a symmetry condition to both $Q^R$ and $Q^I/k$ at $k = 0$. Although the exact $Q^I/k$ is symmetric it is not smooth, whereas the interpolated function is smooth. The symmetry condition in the interpolation controls the smoothness of $Q^I/k$ at whereas symmetry is enforced by evaluating the GAFs at the absolute value of $k$. It is shown that the symmetry, i.e. smoothness, condition on $Q^I/k$ may not be justified in all cases depending on the approximation used to calculate the kernel functions and the selection of reduced frequencies. The effect of this condition on the solution to the flutter equation is usually insignificant. On the other hand, it is shown that failure to apply the symmetry and smoothness condition on $Q^R$ in the case of the *g*-method has a significant effect on the solution to the flutter equation in cases involving divergence.

The generalised aeroelastic analysis method (GAAM) proposed by Edwards[7] solves Equation (1) directly and is therefore a suitable reference solution for evaluating the approximate methods. This method does not use derivatives or interpolated values of the GAFs, at the cost of multiple evaluations of the GAFs using a generalised doublet lattice method.

## 2.0 DERIVATION

The aim of this derivation is to determine the limiting value of $Q^I/k$ as $k$ approaches zero. The derivation is done for the DLM only, but the essential conclusions apply to any subsonic collocation method that uses the kernel functions.

The limiting value of the quotient is simply the derivative of $Q^I$ with respect to $k$ at $k = 0$. However, unless the geometry is normalised by the reference length, the reduced frequency does not have significance at all levels of the DLM and it is more convenient to take the derivative with respect to the wave number. Only the planar case is considered, however, the non-planar case can be treated in a similar way.

$$\lim_{k=0}\frac{Q^I}{k}=\left(\frac{\mathrm{d}Q^I}{\mathrm{d}k}\right)_{k=0}=\frac{1}{b}\left(\frac{\mathrm{d}Q^I}{\mathrm{d}\omega_r}\right)_{\omega_r=0} \qquad \ldots (8)$$

The generalised forces are determined as area integrals of the pressure distribution, which in turn is solved from the downwash equation. The downwash equation reads

$$\{w\}=[\mathbf{D}]\{C_p\} \qquad \ldots (9)$$

Differentiating this expression with respect to wave number and making the appropriate substitutions for zero frequency leads to the following expressions for the steady pressure distribution and the derivative of the imaginary part of the pressure distribution with respect to wave number:

$$\left\{C_p^R\right\}=\left[\mathbf{D^R}\right]^{-1}\left\{w^R\right\} \qquad \ldots (10)$$

$$\frac{\mathrm{d}\left\{C_p^I\right\}}{\mathrm{d}\omega_r}=\left[\mathbf{D^R}\right]^{-1}\left(\left\{w^I\right\}-\frac{\mathrm{d}\left[\mathbf{D^I}\right]}{\mathrm{d}\omega_r}\left\{C_p^R\right\}\right) \qquad \ldots (11)$$

The limiting value of $Q^I/k$ at $k = 0$ is found by integrating the derivative of the imaginary part of the pressure distribution over the surface area of the configuration. It remains to determine the derivative of the imaginary part of the downwash matrix. The planar part of the incremental downwash factor is given in Refe. 4 (after substituting $\omega_r$ for $\omega/U$) as:

$$D_{1rs}=\frac{\Delta x_s}{8\pi}\int_{-e}^{e}\frac{\left\{K_1\exp\left[-i\omega_r\left(\bar{x}-\bar{\eta}\mathrm{Tan}\lambda_s\right)\right]-K_{10}\right\}T_1}{r_1^2}\mathrm{d}\eta \qquad \ldots (12)$$

https://doi.org/10.1017/S0001924000000749 Published online by Cambridge University Press

The derivative of the downwash factor with respect to wave number at zero frequency is

$$\frac{dD_{1rs}}{d\omega_r} = \frac{\Delta x_s}{8\pi}\int_{-e}^{e} \frac{\left\{\frac{dK_1}{d\omega_r} - i\left(x-\eta \mathrm{Tan}\lambda_s\right)K_{10}\right\}T_1}{r_1^2}d\eta \qquad \ldots (13)$$

The integral for the derivative of the downwash factor is evaluated in the same way as the integral for the incremental downwash. The kernel numerator is given in Ref. 4 as:

$$K_1 = -I_1 - \left(\exp\left(-ik_1u_1\right)\right)Mr_1 / R\left(1+u_1^2\right)^{1/2} \qquad \ldots (14)$$

where

$$R = \left[\left(\bar{x}-\bar{\eta}\mathrm{Tan}\lambda_s\right)^2 + \beta^2 r_1^2\right]^{1/2} \qquad \ldots (15)$$

$$u_1 = \left(MR - \bar{x} + \bar{\eta}\mathrm{Tan}\lambda_s\right)/\beta^2 r_1 \qquad \ldots (16)$$

$$I_1 = \int_{u_1}^{\infty}\left(1+u^2\right)^{-3/2}\exp\left(-ik_1u\right)du \qquad \ldots (17)$$

Noting the relationship between $k_1$ and $\omega_r$, the derivative of the kernel numerator with respect to $\omega_r$ at zero frequency is:

$$\frac{dK_1}{d\omega_r} = r_1\left(-\frac{dI_1}{dk_1} + iu_1Mr_1 / R\left(1+u_1^2\right)^{1/2}\right) \qquad \ldots (18)$$

The derivative of $I_1$ with respect to $k_1$ at zero frequency is:

$$\frac{dI_1}{dk_1} = \int_{u_1}^{¥} -iu\left(1+u^2\right)^{-3/2}du = -i\left(1+u_1^2\right)^{-1/2} \qquad \ldots (19)$$

Through Equations (11), (13) and (18) it can be seen that $Q^I/k$ behaves like $dI_1/dk_1$ at low frequencies. Differentiating $I_1$ twice with respect to $k_1$ yields

$$\frac{d^2I_1}{dk_1^2} = -\int_{u_1}^{\infty} u^2\left(1+u^2\right)^{-3/2}\exp\left(-ik_1u\right)du \qquad \ldots (20)$$

Setting $\mu = k_1u$ and taking the limit as $k_1$ approaches zero from the positive side yields

$$\lim_{k_1\to 0^+}\left(\mathrm{Im}\left(\frac{d^2I_1}{dk_1^2}\right)\right) = -\int_0^{\infty}\frac{\mathrm{Sin}\mu}{ì}d\mu = -\pi/2 \qquad \ldots (21)$$

The slope of $dI_1/dk_1$, and consequently the slope of $Q^I/k$, is therefore not generally zero at zero frequency.

## 3.0 IMPLEMENTATION

The formulae derived above were implemented in a doublet lattice code in which the real and imaginary parts of the downwash matrix are stored as two separate real matrices and the real and imaginary parts of the downwash and the pressure distribution are also stored in separate real matrices. The code was modified to do the following at zero reduced frequency:

- Replace the imaginary part of the downwash by $\{w^I\}$ instead of setting it to zero
- Replace the imaginary part of the downwash matrix by its derivative with respect to $\omega_r$ instead of setting it to zero
- Solve the pressure coefficient distribution and its derivative with respect to $\omega_r$ from Equations (10) and (11)
- Divide the derivative of the pressure coefficient distribution with respect to $\omega_r$ by the reference length to obtain the derivative respect to $k$

The output for a zero reduced frequency consists of $Q^R$ and the limiting value of $Q^I/k$.

It was found that the unsteady values for $Q^I/k$ do not approach the limiting value. The reason lies in the fact that the integral $I_1$ is computed from an exponential series approximation in the DLM. This integral cannot be evaluated analytically. It is first integrated by parts to obtain

$$I_1 = \exp\left(-ik_1u_1\right)\left(1-\frac{u_1}{\sqrt{1+u_1^2}}\right) - ik_1\int_{u_1}^{\infty}\exp\left(-ik_1t\right)\left(1-\frac{t}{\sqrt{1+t^2}}\right)dt \qquad \ldots (22)$$

An exponential series approximation, which is valid only for non-negative $t$,

$$1-\frac{t}{\sqrt{1+t^2}} \approx \sum_{k=1}^{n} a_k\exp\left(-b_kt\right) \qquad \ldots (23)$$

is then introduced[8] to obtain

$$I_1 \approx \exp\left(-ik_1u_1\right)\left(1-\frac{u_1}{\sqrt{1+u_1^2}}\right) - ik_1\int_{u_1}^{\infty}\exp\left(-ik_1t\right)\sum_{k=1}^{n}a_k\exp\left(-b_kt\right)dt = \exp\left(-ik_1u_1\right)\left\{\begin{array}{l}\left(1-\frac{u_1}{\sqrt{1+u_1^2}}\right)\\ -ik_1\sum_{k=1}^{n}\frac{a_k\exp\left(-b_ku_1\right)}{ik_1+b_k}\end{array}\right\} \qquad \ldots (24)$$

The derivative of this expression, as well as the corresponding expression for negative $u_1$, with respect to $k_1$ at zero frequency is:

$$\frac{dI_1}{dk_1} = -i|u_1|\left\{\left(1-\frac{|u_1|}{\sqrt{1+u_1^2}}\right)+\sum_{k=1}^{n}\frac{a_k}{b_k}\exp\left(-b_k|u_1|\right)\right\} \qquad \ldots (25)$$

The expression in Equation (25) could be used instead of Equation (19) to obtain a smooth matching of the unsteady results to the limiting values.

## 4.0 RESULTS AND DISCUSSION

The imaginary parts of the generalised forces associated with the first two modes of the BAH wing[9] were calculated using parabolic approximations to the kernel numerators in the spanwise integration and using the L11 series in the kernel evaluation. This method is similar to the standard DLM option in MSC/NASTRAN and is also referred to as the standard DLM in what follows. The GAFs are plotted against reduced frequency in Fig. 1. The empty symbols represent the results at the six reduced frequencies used in the MSC/NASTRAN example HA145B(6), *viz* 0·001, 0·05, 0·1, 0·2, 0·5 and 1·0. The solid symbols represent the limiting values at zero frequency calculated using Equation (19). The solid lines represent results calculated with a fine frequency resolution and the broken lines the interpolated values using the MSC/NASTRAN interpolation scheme. There is a large discrepancy between the limiting

https://doi.org/10.1017/S0001924000000749 Published online by Cambridge University Press

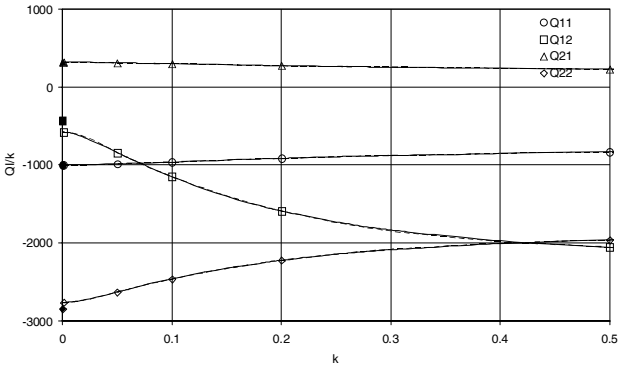



Figure 1. BAH wing generalised forces calculated using the standard DLM and interpolated with the symmetry condition applied.

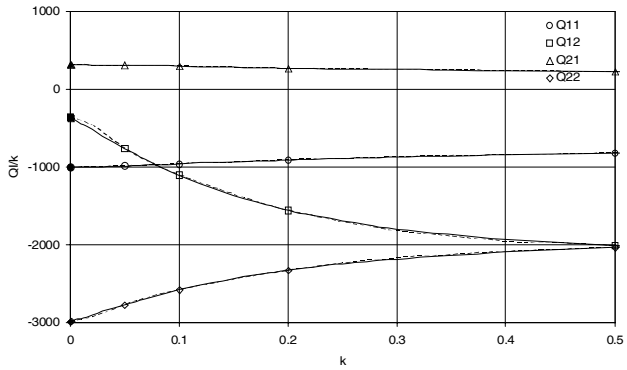



Figure 2. BAH wing generalised forces calculated using the quartic DLM and interpolated with the symmetry condition applied.

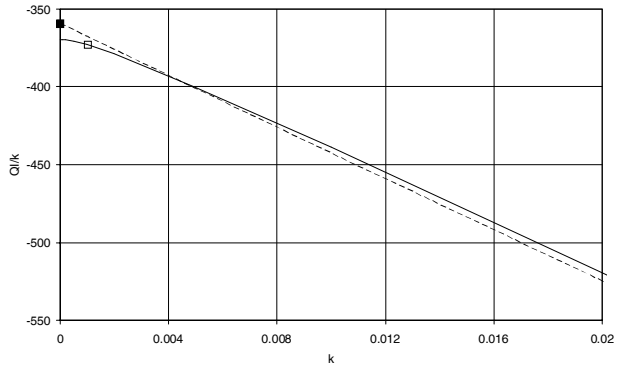



Figure 3. Detail low frequency behaviour of $Q_{1,2}$, calculated using the quartic DLM.

values and the unsteady results for two of the GAFs, whereas the interpolated results closely match the calculated unsteady results. The GAFs that approach the limiting values at zero frequency are associated with the pressure distribution of the first mode, which is almost purely bending and therefore approaches zero at zero frequency. It can be seen from Equation (11) that the derivative of the downwash matrix would not affect the limiting values of these GAFs.

Figure 2 shows the same data as Fig. 1, but calculated using quartic approximations to the kernel numerators in the spanwise integration and using the D12.1 series in the kernel evaluation. This method is similar to the quartic DLM option in MSC/NASTRAN

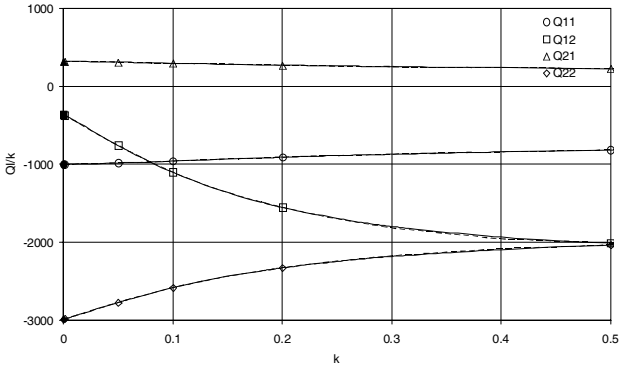



Figure 4. BAH wing generalised forces calculated using the quartic DLM and interpolated without the symmetry condition.

and is referred to as the quartic DLM in what follows. In this case the discrepancy between the limiting values and the unsteady results is small for all GAFs, but the interpolation quality is reduced for two out of the four generalised force terms. The ones that are satisfactorily interpolated are once again those associated with the pressure distribution of the first mode. On this figure it is not evident that the slope of $Q^I/k$ goes to zero at zero frequency, however, it merely happens over a smaller frequency range as shown in Fig. 3.

Figure 4 shows the same data as in Fig. 3. In this case the interpolation was based on the limiting values at zero frequency and the unsteady values at the highest five reduced frequencies. The symmetry condition was not applied in the interpolation and the interpolation quality is improved significantly.

The reduced frequency range over which the slope of $Q^I/k$ goes to zero depends on the magnitude of the $b_k$ terms in the series approximation in Equation (23). The smallest bk in the L11 series is 0·372 and in the D12.1 series it is 0·0181, which explains the features of Figs 1 to 4.

## 5.0 BAH WING EXAMPLE

A quartic doublet lattice method was used to calculate the GAFs for the first five modes using the panelling scheme of Ref. 6. The modeshapes, modal masses and frequencies of the first five normal modes were also taken from Ref. 6. Generalised aerodynamic forces were calculated at 15 reduced frequencies, *viz* 5, 2·5, 2, 1·8, 1·6, 1·4, 1·2, 1·0, 0·8, 0·6, 0·4, 0·3, 0·2, 0·1 and 0·0. Spline interpolation was used to interpolate GAFs for the flutter solution. The interpolation was done on $Q^R$ and $Q^I$. A natural spline was always specified for $Q^I$, implying a symmetry condition on $Q^I/k$ at $k = 0$. The real parts of the roots of the flutter equation were always normalised as is customary for real roots in order to show the transition from oscillatory to non-oscillatory roots clearly, i.e.

$$g = \frac{2\,\mathrm{Re}(p)b}{\ln(2)U} \qquad \ldots (26)$$

The solution of Rodden, Harder and Bellinger's form of the *p-k* flutter equation over the speed range 0 to 2,000fts$^{-1}$ is shown in Fig. 5. A symmetry condition was enforced on the real part of the GAFs by specifying a zero slope at $k = 0$ in the spline fit. The frequency of the first mode goes to zero at 1,451fts$^{-1}$, where it divides into two stable real roots. One root becomes more stable with increasing speed whereas the other one becomes less stable and becomes unstable at 1,658fts$^{-1}$.

The solution of the *g*-method formulation with the real part of d$Q$/d$k$ forced to be zero at $k = 0$ in the spline interpolation is shown in

https://doi.org/10.1017/S0001924000000749 Published online by Cambridge University Press

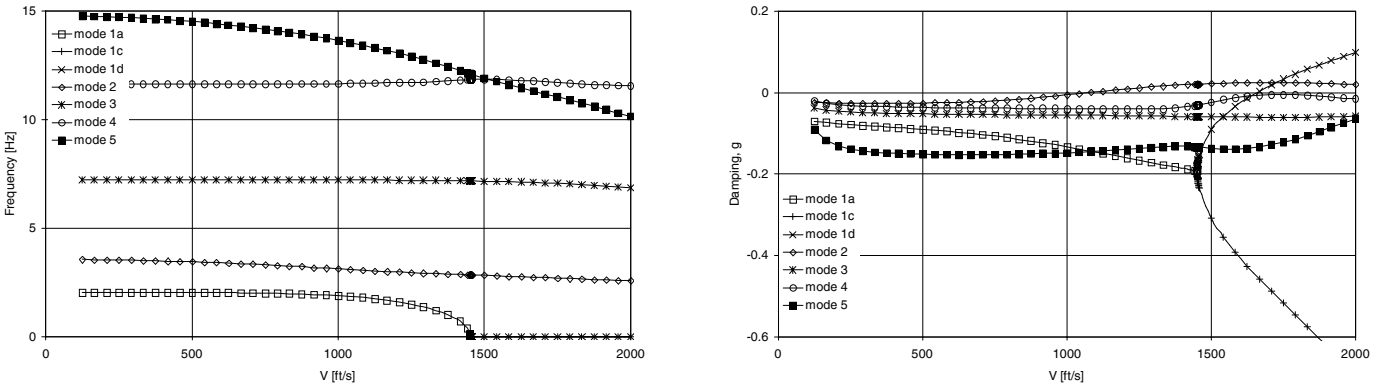



Figure 5. Solution of Rodden, Harder and Bellinger's form of the *p-k* flutter equation.

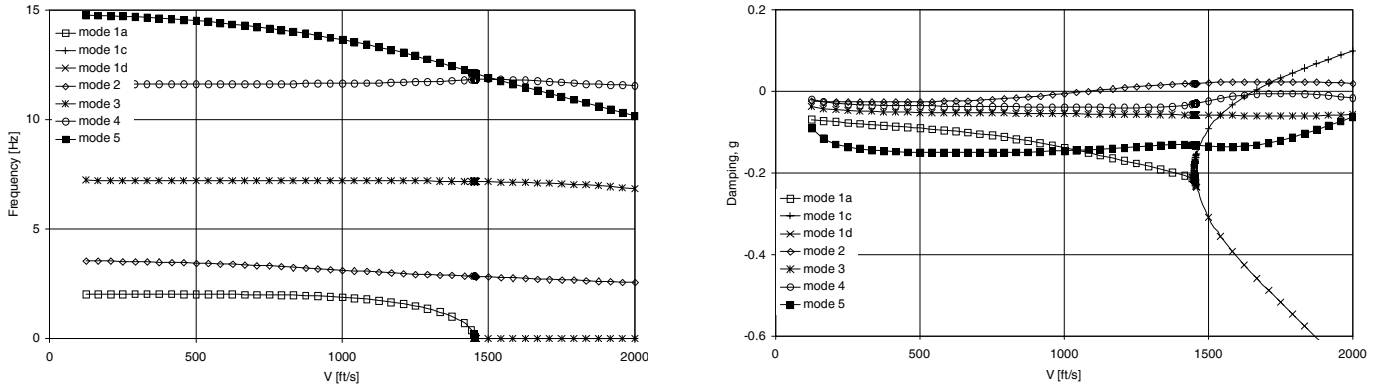



Figure 6. *g*-method solution with the real part of d*Q*/d*k* forced to be zero at $k = 0$.

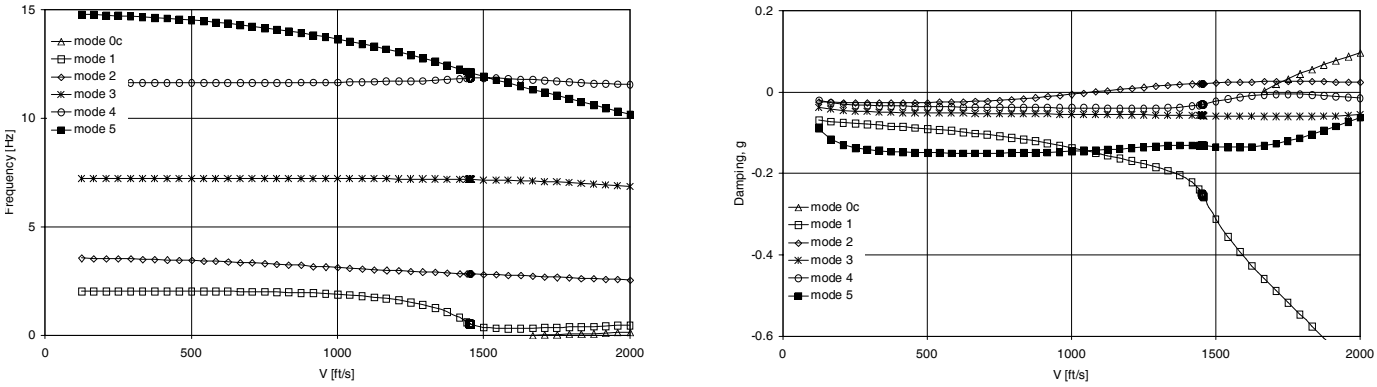



Figure 7. *g*-method solution with the real part of d*Q*/d*k* not forced to be zero at $k = 0$.

Fig. 6. The solution is similar to that of Rodden, Harder and Bellinger's form. The only obvious difference is that the frequency of the first mode does not go to zero at the origin of the real roots. The oscillatory root joins the more stable real root at a speed of 1,453fts$^{-1}$. The speed at which the real roots appear as well as the divergence speed match those predicted by Rodden, Harder and Bellinger's form.

The solution of the *g*-method formulation with the real part of d*Q*/d*k* not forced to be zero at $k = 0$ in the spline interpolation is shown in Fig. 7. In this case the frequency of mode 1 cannot go to zero except if $p = 0$ because of reasons mentioned earlier. The low frequency, highly damped solutions for mode 1 at the higher speeds actually correspond to the more stable real root in the previous solution. The additional low frequency root that appears at $p = 0$ at the divergence speed corresponds to the unstable real root of the previous solution.

https://doi.org/10.1017/S0001924000000749 Published online by Cambridge University Press

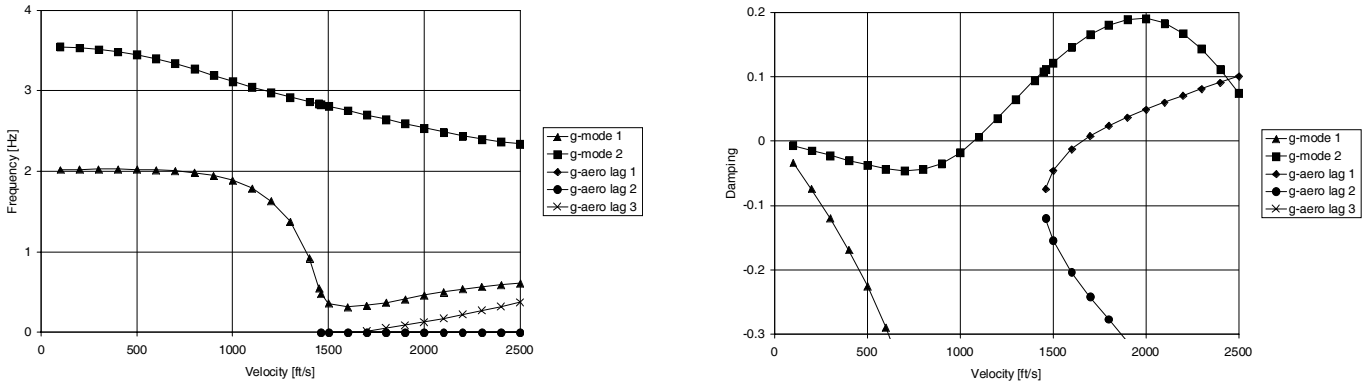



Figure 8. *g*-method solution for comparison with Ref. 3.

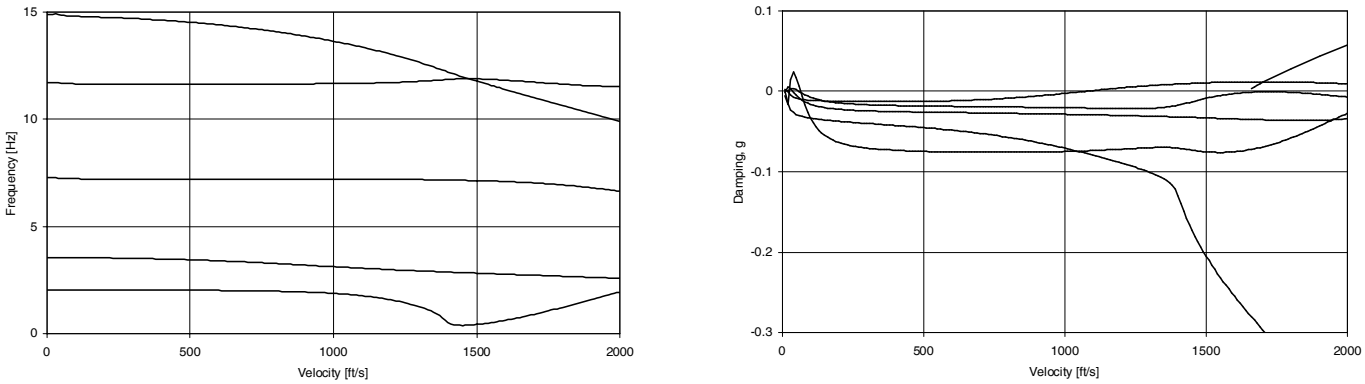



Figure 9. GAAM solution.

The solution presented by Chenfts[3] actually consists of the solution in Fig. 7, plus the real roots from Fig. 5. That is, the solution of Equation (6) with the slope of $Q^R$ not forced to go to zero at $k = 0$, plus the solution of Equation (7). It should be noted that the normalisation in Figs 5 to 7 differs from that used in Ref. 3. In order to facilitate the comparison with Ref. 3, a solution constructed in this way and normalised and scaled as in Ref. 3 is shown in Fig. 8. The general features of the solutions correlate well, with the main difference being the rate at which the frequencies of structural mode 1 and aero lag mode 3 increase after the divergence speed. This rate is very sensitive to the interpolation and more information on how the solution in Ref. 3 was generated would be required to obtain a better correlation. In Ref. 3 aero lag root 3 was treated as a real root for normalisation purposes over a small speed range after its appearance and thereafter as an oscillatory root, which explains the jump in damping value. In the present results it was treated as an oscillatory root throughout and the normalised damping values are too high to appear on these graphs.

The GAAM solution using the D12.1 series approximation in a quartic DLM is shown in Fig. 9. This solution differs from the *p-k* and *g*-method results in Figs 5 and 6 in that the frequency of mode 1 does not go to zero, and that the divergence root is not linked to mode 1 but originates on the positive real axis close to the origin of the *p*-plane at a speed just above the divergence speed. The behaviour of mode 1 corresponds to the erroneous *g*-method solution of Fig. 7, however, the divergence root is a real root in the GAAM solution whereas it is an oscillatory root in the erroneous *g*-method solution.

Edwards[7] reported that the divergence root appears on the negative real axis below the divergence speed. This difference is due to the aerodynamic poles introduced by the exponential series in the kernel function evaluation. For the L11 series used by Edwards, these poles are much further from the origin along the negative real axis that those of the D12.1 series.

## 6.0 CONCLUSION

Expressions were derived for calculating the limiting value of $Q^I/k$ at $k = 0$ directly from the DLM rather than from an interpolation performed on results at non-zero reduced frequencies. Expressions were derived both for the exact and approximated integral part of the kernel numerator. Apart from the application to the flutter equation considered here, this procedure may also be used to obtain aerodynamic coefficients for quasi-static analysis of free-flying elastic flight vehicles[10].

The low frequency behaviour of the imaginary parts of the generalised forces calculated by the DLM was investigated with respect to a symmetry condition imposed in the interpolation of $Q^I/k$, as is done in MSC/NASTRAN. It was illustrated that the symmetry condition is not always appropriate. The desirability of imposing the symmetry condition is influenced by the series approximation used in the evaluation of the kernel numerators as well as the choice of reduced frequencies. Applying the symmetry condition inappropriately compromises the interpolation accuracy slightly, but the effect on the flutter analysis results is small.

In the case of the *g*-method of flutter solution it is important to enforce a symmetry condition on the real part of the GAFs, especially in cases involving divergence. The differences between the *p-k* results and the *g*-method results reported in Ref. 3 were shown to be mostly due to the inconsistent treatment of the low-frequency aerodynamics.

https://doi.org/10.1017/S0001924000000749 Published online by Cambridge University Press

## REFERENCES


1. HASSIG, H.J. An approximate true damping solution of the flutter equation by determinant iteration, *J Aircr*, 1971, **8**, (11), pp 885-889.
2. RODDEN, W.P., HARDER, R.L. and BELLINGER, E.D. Aeroelastic addition to NASTRAN, 1979, NASA CR 3094.
3. CHEN, P.C. A damping perturbation method for flutter solution: the *g*-method, Proceedings of the International Forum on Aeroelasticity and Structural Dynamics, 1999, Part 1, NASA/CP-1999-209136/PT 1, Hamptom, VA, pp 433-441.
4. RODDEN, W.P., GIESING, J.P. and KALMAN, T.P. New developments and applications of the subsonic doublet-lattice method for nonplanar configurations, 1971, AGARD Conference Proceedings, CP-80-71, Part II, No 4.
5. RODDEN, W.P., TAYLOR, P.F. and MCINTOSH, S.C. Further refinement of the nonplanar aspects of the subsonic doublet-lattice lifting surface method, 1996, ICAS Conference Proceedings, Paper 96-2.8.2.
6. RODDEN, W.P. and JOHNSON, E.H. *MSC/NASTRAN Version 68 Aeroelastic Analysis User's Guide*, March 1994, MacNeal-Schwendler Corporation.
7. EDWARDS, J.W. and WIESEMAN, C.D. Flutter and divergence analysis using the generalised aeroelastic analysis method, 2003Paper presented at the International Forum on Aeroelasticity and Structural Dynamics 2003, Amsterdam, The Netherlands.
8. DESMARAIS, R.N. An accurate and efficient method for evaluating the kernel of the integral equation relating pressure to normalwash in unsteady flow, ??date??, AIAA 82-0687.
9. BISPLINGHOFF, R.L., ASHLEY, H. and HALFMAN, R.L. *Aeroelasticity*, 1955, Addison-Wesley Publishing Co.
10. DYKMAN, J.R. and RODDEN, W.P. Structural dynamics and quasistatic aeroelastic equations of motion, *J Aircr*, 2000, **37**, (3), pp 538-542.


https://doi.org/10.1017/S0001924000000749 Published online by Cambridge University Press